Title

PapRIV, a BV-2 microglial cell activating quorum sensing peptide.

Journal

Scientific reports, 11(1)

ISSN

2045-2322

Authors

Janssens, Yorick
Debunne, Nathan
De Spiegeleer, Anton
et al.

Publication Date

2021-05-01

DOI

10.1038/s41598-021-90030-y

Peer reviewed

scientific reports

Check for updates

OPEN

PapRIV, a BV-2 microglial cell activating quorum sensing peptide

Yorick Janssens[1], Nathan Debunne[1], Anton De Spiegeleer[1,2,3], Evelien Wynendaele[1], Marta Planas[4], Lidia Feliu[4], Alessandra Quarta[5,6], Christel Claes[7], Debby Van Dam[8,9], Peter Paul De Deyn[8,9], Peter Ponsaerts[5,6], Matthew Blurton-Jones[7,10,11] & Bart De Spiegeleer[1]✉

Quorum sensing peptides (QSPs) are bacterial peptides produced by Gram-positive bacteria to communicate with their peers in a cell-density dependent manner. These peptides do not only act as interbacterial communication signals, but can also have effects on the host. Compelling evidence demonstrates the presence of a gut-brain axis and more specifically, the role of the gut microbiota in microglial functioning. The aim of this study is to investigate microglial activating properties of a selected QSP (PapRIV) which is produced by *Bacillus cereus* species. PapRIV showed in vitro activating properties of BV-2 microglia cells and was able to cross the in vitro Caco-2 cell model and reach the brain. In vivo peptide presence was also demonstrated in mouse plasma. The peptide caused induction of IL-6, TNFα and ROS expression and increased the fraction of ameboid BV-2 microglia cells in an NF-κB dependent manner. Different metabolites were identified in serum, of which the main metabolite still remained active. PapRIV is thus able to cross the gastro-intestinal tract and the blood–brain barrier and shows in vitro activating properties in BV-2 microglia cells, hereby indicating a potential role of this quorum sensing peptide in gut-brain interaction.

Abbreviations

QSP	Quorum sensing peptide
ICR-CD-1	Institute for Cancer Research, Caesarean Derived-1
BBB	Blood–brain barrier
ASD	Autism spectrum disorder
AD	Alzheimer's disease
PD	Parkinson's disease
ROS	Reactive oxygen species
FBS	Fetal bovine serum
NEAA	Non-essential amino acids
TMB	Tetramethylbenzidine
SEM	Standard error on mean
MMP-9	Matrix-metalloprotease 9

Quorum sensing is a cell–cell communication system used by micro-organisms to sense the density of their peers by secreting quorum sensing molecules. By using this system, gene expression is regulated in response to the microbial cell density. A variety of cell functions such as expression of virulence factors, biofilm formation, competence and sporulation are controlled by this communication system[1]. The process of quorum sensing is not only limited to bacteria, but it is also observed in other microbial cell types such as yeasts and fungi[2,3]. Different types

[1]Drug Quality and Registration (DruQuaR) Group, Faculty of Pharmaceutical Sciences, Ghent University, Ghent, Belgium. [2]Department of Geriatrics, Faculty of Medicine and Health Sciences, Ghent University Hospital, Ghent, Belgium. [3]Unit for Molecular Immunology and Inflammation, VIB-Center for Inflammation Research, Zwijnaarde, Belgium. [4]LIPPSO, University of Girona, Girona, Spain. [5]Laboratory of Experimental Hematology, University of Antwerp, Wilrijk, Belgium. [6]Vaccine and Infectious Disease Institute (Vaxinfectio), University of Antwerp, Wilrijk, Belgium. [7]Sue and Bill Gross Stem Cell Research Center, University of California, Irvine, CA 92696, USA. [8]Laboratory of Neurochemistry and Behavior, Institute Born-Bunge, University of Antwerp, Wilrijk, Belgium. [9]Department of Neurology and Alzheimer Center, University of Groningen, University Medical Center Groningen, Groningen, The Netherlands. [10]Department of Neurobiology and Behavior, University of California, Irvine, CA 92697, USA. [11]Institute for Memory Impairments and Neurological Disorders, University of California, Irvine, CA 92696, USA. ✉email: Bart.DeSpiegeleer@UGent.be

of quorum sensing molecules in bacteria exist: Gram-negative bacteria mostly use *N*-acyl homoserine lactones, while Gram-positive bacteria produce oligopeptides for their communication, which are called quorum sensing peptides (QSPs)[4–6]. Other quorum sensing molecules, such as furan borate derivatives and other miscellaneous molecules, exist as well[7,8]. The QSPs are produced as large pro-peptides, secreted outside the microbial cell by ATP-binding cassette transporters, whilst hydrolyzed to the active QSP. They then interact with neighboring microbial cells via two possible mechanisms: either with membrane-located receptors (mainly histidine kinases) for signal transduction, or directly with cytoplasmic sensors (e.g. the RNPP family) after being transported over the microbial cell membrane by oligopeptide permeases[4]. The QSPs are chemically and microbiologically described in the Quorumpeps database which currently contains over 350 different peptides[9]. Recently, it has been found that these peptides not only influence micro-organisms but can also affect cells of the host. For example, QSPs promote tumor cell invasion and angiogenesis in vitro, thereby promoting epithelial-mesenchymal transition and metastasis[10,11]. Mast cells are able to sense CSP-1, a QSP produced by *Streptococcus pneumoniae*, hereby triggering degranulation and the release of antibacterial mediators[12]. In vitro research also suggests that QSPs influence host muscle wasting diseases[13]. QSPs can also cross the blood–brain barrier and thus potentially influence brain cells[14]. Indeed, an in vitro screening of 85 different QSPs indicated that some peptides have the ability to exert biological effects on different types of brain cells[15].

Microbial dysbiosis is observed in a variety of neurodevelopmental- , neurodegenerative- and psychiatric disorders such as autism spectrum disorders (ASD), schizophrenia, Alzheimer's disease (AD), major depressive disorder, and Parkinson's disease (PD)[16–24]. A causal relationship between these gut microbiota and brain disorders is becoming increasingly evident: fecal transfer of human ADHD, PD and AD patients aggravates symptoms in in vivo mice models of these disorders[25–27]. Alternatively, transfer of a 'healthy' microbiota reduced amyloid and tau pathology in an AD mouse model[28]. This microbiota-brain association is considered part of a bi-directional communication pathway between the gut and brain, called the gut-brain axis[29]. Various communication routes including the immune system, the vagus nerve, the enteric nervous system and microbial metabolites, such as short chain fatty acids, amino acids and peptidoglycans are proposed as mediators of this axis, but many factors remain largely unknown[30]. Peptides also contribute in this microbiome-to-brain signaling as interactions of the microbiota with gut hormones and entero-endocrine peptides are observed[31]. Microglial dysfunction and activation is present in a variety of neuronal conditions such as AD, ASD, multiple sclerosis, PD and amyotrophic lateral sclerosis[25,32–37]. Germ-free mice display global defects in microglia with altered cell proportion and an immature phenotype, indicating that the gut microbiome plays a role in microglial maturation and functioning during development and aging[32,38]. When transplanting faeces from human AD or PD patients to in vivo mouse models, cognitive and physical impairments are aggravated, which is partly mediated by enhanced microglial activation in the brain[25,26]. Prebiotics are already being developed that target this gut microbiota-microglial axis for the treatment of AD. Sodium oligomannate, which will shortly be studied as an investigational drug in a large AD phase III global clinical trial, suppresses gut dysbiosis together with the associated phenylalanine/isoleucine accumulation in an AD mouse model, resulting in reduced microglial activation, amyloid-β deposition, tau phosphorylation and amelioration of cognitive impairment[39]. All these studies indicate that the gut microbiota can influence neurodevelopmental-, neurodegenerative- and psychiatric disorders by regulation of microglia cells. However, the exact mechanisms on how the gut microbiota influence these microglial cells remains largely unknown.

After a screening of 85 different QSPs on different brain cell types[15], repeat testing of PapRIV consistently demonstrated its in vitro microglia activating properties. PapRIV is a heptapeptide (SDLPFEH) originating from the *Bacillus cereus* group, which comprises a number of highly related species. The *B. cereus* group (sensu lato), which is widespread in soil and food, is generally considered as an opportunistic human pathogen because it triggers food-borne gastroenteritis and some non-gastro-intestinal infections like pneumonia and endophthalmitis, as well as infections resembling to anthrax. However, presence of *B. cereus* in the human gastro-intestinal tract is already been demonstrated without provoking illness, indicating the symbiotic life cycle of this species[40]. The diseases associated with *B. cereus* are caused by several cytotoxic products, which are produced by activation of the PlcR quorum sensing system. The PapRIV peptide is translated as a 48- amino acid polypeptide which is secreted out of the cell under influence of the N-terminal signaling sequence and extracellularly processed by NprB proteases to form the active PapRIV heptapeptide[41,42]. The concentrations used in these in vitro microbiological activity studies ranged between 1 and 100 μM[42]. Instead of binding to a membrane-coupled sensor receptor and activating a two-component signaling system, PapRIV binds directly to its regulatory cytoplasmatic PlcR protein after being imported in the cell by the ABC transporter family member Opp (oligopeptide permease). This binding activates the regulatory PlcR protein resulting in a conformational change, binding to the promotor region and transcriptional activation of PlcR target genes[43,44]. Activation of this quorum sensing system induces production of extracellular virulence factors, such as enterotoxins, haemolysins, cytotoxins and various degradative enzymes (e.g. proteases). However, the effects of the peptide itself towards the host remained unexplored. Here, we demonstrate for the first time microglial activating properties of a QSP, indicating the potential of these peptides as mediators of the gut-brain-microglia axis.

Results

PapRIV is able to reach the circulation and cross the blood–brain barrier. PapRIV showed a low transport rate across the Caco-2 monolayer with a P_{app} of $1.37 \pm 0.21 \times 10^{-9}$ cm/s and is thus potentially able to cross the intestinal wall and reach the circulation (Fig. 1a and Supplementary Fig. S1). Indeed, PapRIV was detected (ie > 1.5 nM) and identified in 4 out of 66 wild type mice plasma samples (Table 1 and Supplementary Fig. S2) which is an extra indication that the peptide is able to cross the gastro-intestinal tract and reach the circulation in vivo. Estimated concentrations were ranging between 1.7 and 19.2 nM. These values are consistent

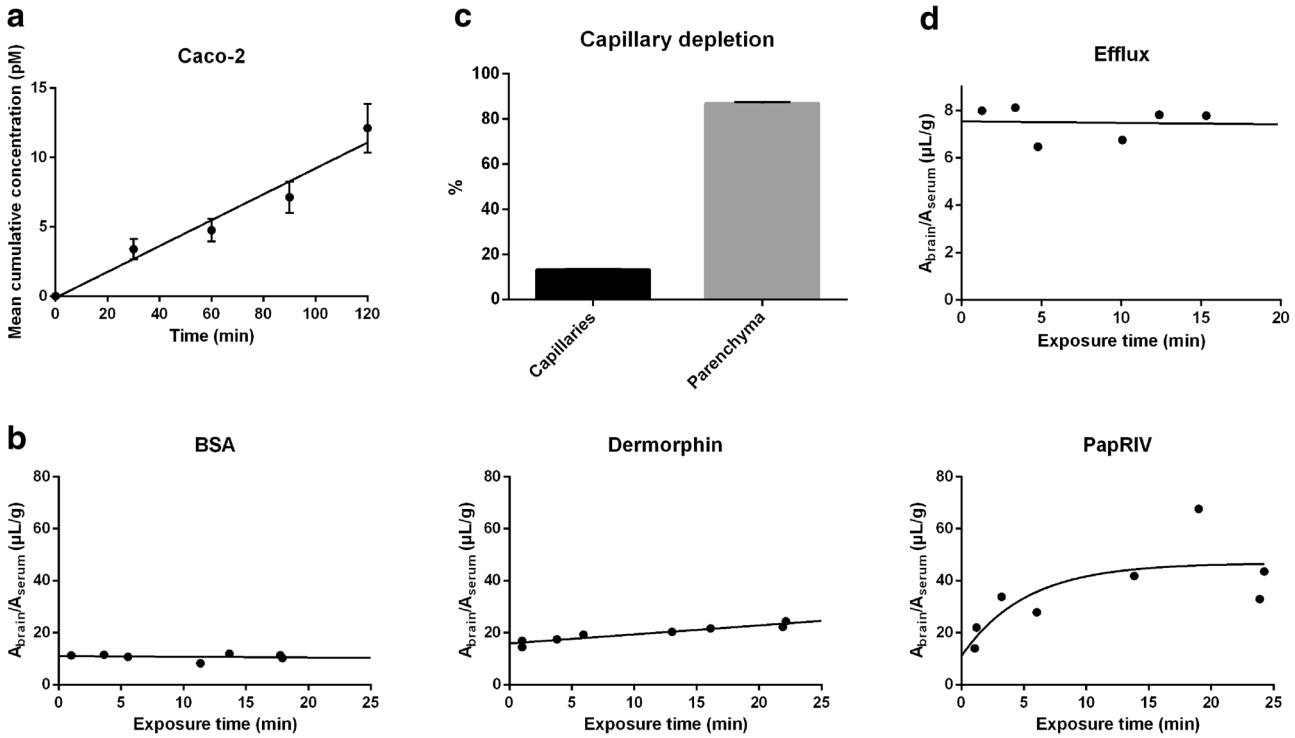

Figure 1. PapRIV passes the Caco-2 monolayer and blood–brain barrier. (**a**) The PapRIV peptide passes the Caco-2 monolayer and accumulates in the acceptor compartment (n = 6). (**b**) Multiple time regression analysis of BSA, Dermorphin and PapRIV across the blood–brain barrier. BSA and Dermorphin, the negative and positive controls respectively, follow a linear model while the PapRIV peptide is following a biphasic model with an initial steep influx followed by a steady state. (**c**) After 10 min, 87% of the peptide reaches the brain parenchyma while 13% remains in the capillaries (n = 2). (**d**) Efflux data of the peptide from the brain to the circulation.

Samples	Parent ions			Daughter ions		
	Theoretical (*m/z*)[a]	Measured (*m/z*)	Δ[b]	Theoretical (*m/z*)[c]	Measured (*m/z*)	Δ[b]
Sample 6	844.3836	844.3639	+ 0.0197	529.2406	529.2471	− 0.0065
	–	–	–	156.0768	156.0856	− 0.0088
Sample 7	844.3836	844.4272	− 0.0436	642.3246	642.3661	− 0.0415
	–	–	–	413.2031	413.2082	− 0.0051
Sample 16	844.3836	844.3892	− 0.0056	529.2406	529.2471	− 0.0065
	845.3859	845.3915	− 0.0056	642.3246	642.3108	+ 0.0138
	846.3883	846.3945	− 0.0063	689.3141	689.3146	− 0.0005
	847.3906	847.3979	− 0.0073	156.0768	156.0802	− 0.0034
	–	–	–	826.3730	826.3615	+ 0.0115
	–	–	–	413.2031	413.2082	− 0.0051
	–	–	–	432.1878	432.1870	+ 0.0008
	–	–	–	285.1194	285.1234	− 0.0040
	–	–	–	560.2715	560.2549	+ 0.0166
Sample 35	844.3836	844.4019	− 0.0183	529.2406	529.2471	− 0.0065
	845.3859	845.4042	− 0.0183	642.3246	642.3329	− 0.0083
	846.3883	846.4072	− 0.0189	156.0768	156.0802	− 0.0034
	847.3906	847.3852	− 0.0054	285.1194	285.1234	− 0.0040
	–	–	–	413.2031	413.2082	− 0.0051
	–	–	–	432.1878	432.2051	− 0.0173
	–	–	–	560.2715	560.2858	− 0.0143
	–	–	–	689.3141	689.3261	− 0.0120

Table 1. Measured parent- and daughter ions in positive mice plasma samples. [a]As determined by 'Isotope Distribution Calculator' (MacCoss Lab, University of Washington, USA). [b]Difference between theoretical and measured *m/z* values. [c]As determined by 'Fragment Ion Calculator'.

	Peptide (^{125}I-)	K_{in} (µL/g × min)	K_1 (µL/g × min)	K (µL/g × min)	Vascular brain distribution volume, V_0 (µL/g)	Tissue brain distribution volume, V_g (µL/g)	Parenchymal fraction (%)	Capillary fraction (%)	k_{out} (min^{-1})
Linear	BSA	− 0.03 ± 0.08 [− 0.23 to 0.18]	N/A	N/A	11.08 ± 0.99 [8.62 to 13.54]	N/A	N/A	N/A	N/A
	Dermorphin	0.35 ± 0.05 [0.23 to 0.46]	N/A	N/A	15.93 ± 0.64 [14.38 to 17.47]	N/A	N/A	N/A	N/A
Biphasic	PapRIV	N/A	6.95 ± 6.25 [0.00 to 22.54]	0	–[a]	35.70 ± 61.73 [0.00 to 189.70]	86.92	13.08	− 0.01 ± 0.05 [− 0.18 to 0.16]

Table 2. Overview of the multiple time regression results of BSA, Dermorphin and PapRIV using both the linear- and biphasic model (mean ± standard error, 95% CI interval between brackets). *N/A* not applicable seen the model applied. [a](V_0): The vascular brain distribution volume V_0 was set to be equal to the V_0 of radio-iodinated BSA obtained in these experiments (11.077 µL/g) (= V_i).

with already reported concentrations of quorum sensing molecules in biofluids (between nM–µM concentration)[6]. Once circulating, the peptide is able to cross the blood–brain barrier based on experiments in the in vivo MTR mice model (Fig. 1b). The pharmacokinetic parameters of PapRIV and of the negative and positive control, respectively BSA and Dermorphin, are given in Table 2. BSA and Dermorphin followed a linear model while the PapRIV peptide displayed a biphasic model with an initial steep influx followed by a steady state situation. PapRIV showed an initial brain influx rate (K_i) of 6.95 µl/(g × min) and can be classified as a peptide with a very high brain influx according to the classification system designed by Stalmans et al.[45]. Based on the capillary depletion experiment, it was observed that 87% of the peptide that is taken up by the brain eventually reached the parenchyma (Fig. 1c; Table 2). Once the peptide enters the brain, no efflux back to the circulation is observed as the k_{out} was not significantly different from zero (Fig. 1d; Table 2). In conclusion, the peptide is able to pass the Caco-2 monolayer, can be detected in mouse plasma and is able to pass the blood–brain barrier and reach the brain where possible effects can be exerted.

PapRIV shows pro-inflammatory effects on BV-2 microglia cells in vitro. The PapRIV peptide showed in vitro pro-inflammatory effects on the microglial BV-2 cell line, an immortalized murine microglial cell line which has proven its suitability for in vitro microglial research and investigation of neuro-inflammation[46–48]. The PapRIV peptide induced the production of the pro-inflammatory cytokines IL-6 and TNFα (Fig. 2a); for IL-6, these changes were also confirmed at the mRNA level by qPCR (Fig. 2b). This induction of pro-inflammatory cytokines was accompanied by an increase of intracellular ROS and an increased fraction of ameboid cells (Fig. 2c-d, Supplementary Fig. S3). Treatment with 1 µg/mL LPS resulted in a fraction of ameboid cells of around ± 50% (data not shown). This microglial activation is mediated by an increased NF-kB nuclear translocation caused by decreasing IκBα levels, an inhibitory protein of NF-kB (Fig. 2e,f). NIK expression was not observed in the cells (data not shown), thus indicating a canonical activation of the NF-kB pathway[49]. By synthesizing an alanine-scan of the sequence, we could identify the crucial amino acids of the peptide to exert its pro-inflammatory effects in the BV-2 microglial cells. When replacing aspartic acid or proline at respectively position 2 and 4 by an alanine residue, the corresponding peptide was not able anymore to induce IL-6 and TNFα production (Fig. 2g). A scrambled control (DEHSFLP), which has the same amino acids as the native sequence but arranged in a random order, also showed no activating properties indicating that the specific sequence of amino acids is important for its function.

Conditioned medium of PapRIV treated BV-2 is toxic for SH-SY5Y neuroblast cells. Treatment of SH-SY5Y neuroblast cells with conditioned medium of BV-2 cells treated with PapRIV caused toxic effects on these neuroblast cells as demonstrated by a significant decreased viability of the cells (Fig. 3a). This effect was not caused by direct actions of the peptide itself on the neuroblast cells as a direct treatment with the peptide caused no significant toxic effects (Fig. 3b). The peptide thus shows indirect neurotoxic effect via microglia activation. PapRIV also showed no significant toxic effects up to 25 µM, as measured by MTT, towards the BV-2 microglia cells (Supplementary Fig. S4).

Different metabolites of PapRIV are formed in serum, brain, liver, kidney and faeces. The metabolization rate of the peptide varied between different biological matrices such as serum, brain tissue, liver tissue, kidney tissue and faeces. The fastest metabolization rate was observed in kidney tissue, with a half-life of only 19.8 min. The half-lives in serum, faeces, liver and brain tissue were respectively 24.8, 89.7, 286 and 523 min while no metabolization was observed in colon tissue (Table 3, Supplementary Fig. S5). Different metabolites of the peptide could be identified. To exclude the possibility of non-enzymatic degradation, the chemical and protease-inactivated homogenate (by pre-heating the homogenate for 5 min at 95 °C) stability of the peptide was determined. Except for kidney tissue, PapRIV remained stable in protease-inactivated homogenates, pointing an enzymatic degradation in serum, liver, brain and faeces (Supplementary Table S1). In protease-inactivated kidney homogenate, approximately 45% of peptide loss after 60 min can be explained by protein interaction with some kidney specific proteins. In serum, six different metabolites were formed. The MS-spectra of the different metabolites formed and the metabolic profiles in different tissues are given in supplementary information

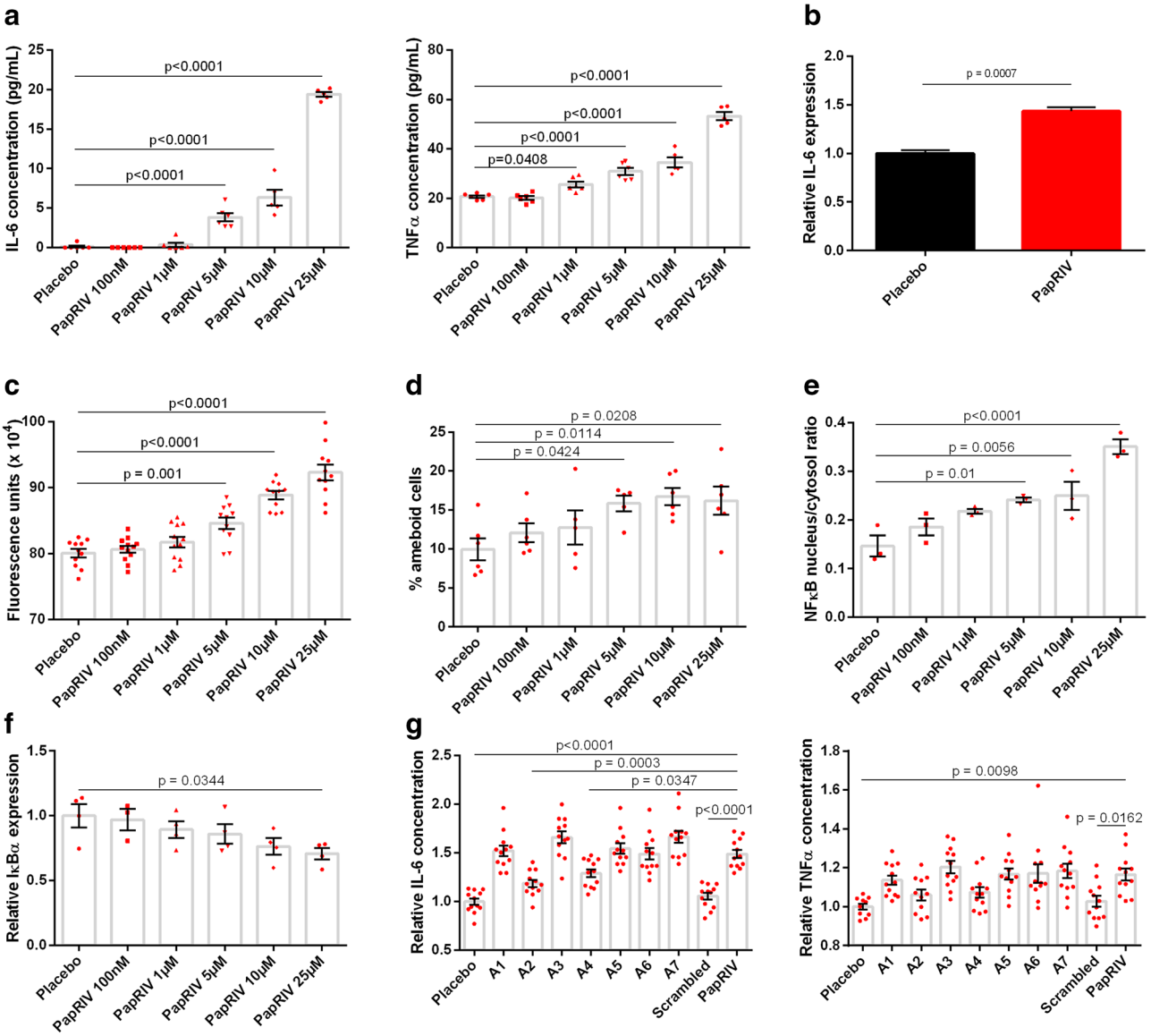

Figure 2. In vitro microglial activation of BV-2 cells by PapRIV. (**a**) IL-6 and TNFα levels increase after increasing concentrations of PapRIV (n = 6). (**b**) IL-6 mRNA expression is increased after treatment with 10 µM PapRIV (n = 6). (Mann–Whitney U test) (**c**) Reactive oxygen species are formed after treatment (n = 12). (**d**) The fraction of ameboid cells, a marker for microglial activation, increased after treatment (n = 6). (**e**,**f**) Activation is mediated by an increased nuclear translocation of NF-kB caused by decreasing IκBα levels (n = 3). (**g**) Critical amino acids are identified by an alanine scan of the native sequence (10 µM, n = 12). Mean ± SEM, One-way ANOVA, post-hoc Dunnett.

(Supplementary Figs. S6, S7). DLPFEH is the main metabolite which is formed in all matrices, metabolization of the native peptide to this metabolite is the main contributor of the low half-lives observed in kidney tissue and serum (Supplementary Fig. S5). Also in faeces, the matrix in which PapRIV is produced by gut bacteria, metabolization to DLPFEH occurred. Since this peptide still contains the two critical amino acids (D and P) at positions 2 and 4, respectively, the question was raised whether this peptide also showed microglial activating properties. As hypothesized, DLPFEH showed similar microglial activating properties as it was also able to induce IL-6 production to the same extent as the native sequence; the other metabolites showed no activity (Fig. 4). Remarkably, SDLPF and DLPF showed no activating properties despite the presence of the two critical amino acids, thereby indicating that the presence of the C-terminal EH sequence is also necessary for the peptide's action.

Discussion

PapRIV, a QSP which is produced by *B. cereus*, showed in vitro pro-inflammatory effects in BV-2 microglia cells. The peptide, which is mainly produced in the gut, is able to transfer across the gastro-intestinal tract and reach the circulation based on the in vitro Caco-2 model. A relatively low but appreciable P_{app} of $1.37 \pm 0.21 \times 10^{-9}$ cm/s is observed. A passive paracellular transport mechanism is suggested, as a comparable P_{app} was observed in the

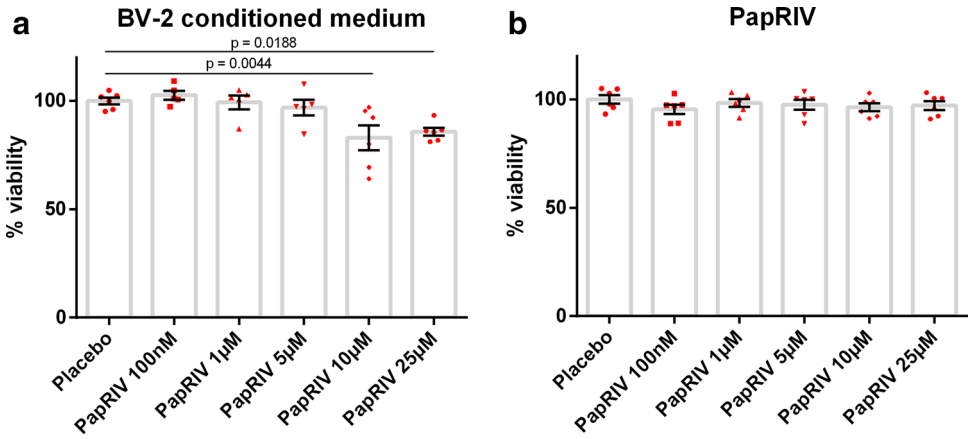

Figure 3. Indirect neurotoxic effects of PapRIV via microglia activation. (**a**) Treatment of SH-SY5Y cells with conditioned medium of PapRIV peptide-treated BV-2 cells is toxic for these neuroblasts (n = 6). (**b**) Direct treatment of SH-SY5Y cells with PapRIV shows no direct toxicity (n = 6). Mean ± SEM, one-way ANOVA, post-hoc Dunnett.

Matrix	$T_{1/2}$ (min)	Metabolites
Serum	24.8	DLPFEH, LPFEH, LPFE, LPF, SDLPF, DLPF
Brain	522.9	DLPFEH, LPFEH
Liver	285.7	DLPFEH, LPFEH
Kidney	19.8	DLPFEH, LPFEH
Faeces	89.7	DLPFEH
Colon	–	–

Table 3. Peptide half-lives and formed metabolites in different biological matrices.

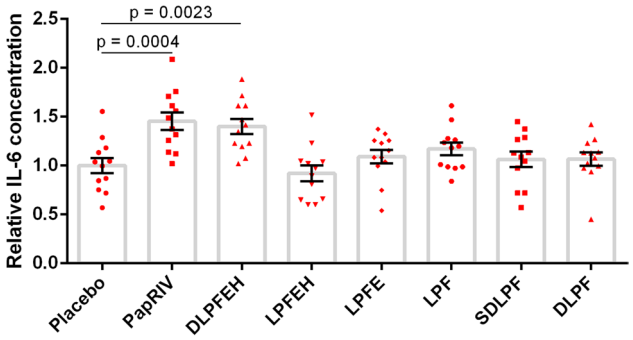

Figure 4. Activating properties of PapRIV metabolites on BV-2 microglia cells (10 µM, n = 12). Mean ± SEM, one-way ANOVA, post-hoc Dunnett.

opposite basolateral-apical direction, as well as at 4 °C (Supplementary Fig. S1). The low P_{app} can be explained by the low mass balance observed (< 2%), indicating that peptide is lost during the experimental timeframe due to either cellular uptake or enzymatic degradation. Indeed numerous brush border membrane peptidases (i.a. aminopeptidases, dipeptidylpeptidase IV) are present on the apical side of the Caco-2 cells which may be responsible for enzymatic degradation of PapRIV during the experimental timeframe[50,51]. The peptide was detected and identified in 4 out of 66 mice plasma samples, with concentrations ranging between approximately 2 (lowest reporting threshold) and 20 nM, while a protein BLAST search demonstrated that the sequence is not present in the mouse proteome and can thus not be the result of proteolytic cleavage of endogenous proteins. The sequence is also not present in common plant proteins, indicating that the observed peptide sequence is not the result of protein cleavage of feed proteins. These mice plasma findings also support the Caco-2 data that the peptide is able to cross the gastro-intestinal tract and reach the circulation in vivo. Unfortunately, the presence of *B. cereus* in the gut microbiota of these mice has not been investigated, making it impossible to

investigate correlations between the presence of *B. cereus* in the gut and PapRIV in plasma. Translationally, the presence of *B. cereus* in the human gastro-intestinal tract has previously already been demonstrated, up to 30% of vegetative cells and 100% of spores can survive gastric passage[52–55]. Gut permeability is also modulated by the intestinal microbiota. For example, expression of epithelial tight junction proteins is downregulated by several intestinal pathogens hereby increasing the permeability of the barrier[56]. The majority of *B. cereus* strains cause food poisoning and produce enterotoxins which are also able to increase vascular permeability[57,58]. Spores are able to adhere in aggregates to both Caco-2 as small intestine gastro-intestinal epithelial cells which triggers germination and the production of enterotoxins; bacterial cells are thus in the proximity of the epithelial barrier facilitating the transport of metabolites[59]. Moreover, the intestinal barrier function is affected in several gastro-intestinal disorders such as IBD, IBS, celiac disease and obesity leading to a 'leaky gut' and an increased flux of luminal compounds towards the circulation[56]. Also in mental disorders such as ASD, ADHD and bipolar disorder, increased serum zonulin and/or claudin-5 levels are observed which is associated with respectively increased intestinal and BBB permeability[60,61].

Once in the circulation, the peptide can reach the blood–brain barrier where it shows a very high brain influx according to the classification system of Stalmans et al.[45]. No significant brain efflux of the peptide was observed. PapRIV is thus able to reach the brain parenchyma where it can exert biological effects.

PapRIV showed in vitro microglia activating properties in BV-2 cells. A significant induction of both IL-6 and TNFα, two pro-inflammatory cytokines, in these cells is observed. These effects were accompanied by a significant increase of ROS. ROS are involved in the continued activation of microglia, even if the activating agent is already removed, a phenomenon called 'reactive microgliosis'[62]. This reactive microgliosis is explained by the presence of a self-amplifying loop: ROS are able to initiate NF-κB nuclear translocation and thus induction of gene transcription of pro-inflammatory mediators, while these pro-inflammatory cytokines consequently can increase ROS production[63]. Whether PapRIV has a direct effect on both factors or that one of both is indirectly affected by the other is yet unclear. In addition, microglia are extremely plastic and undergo a variety of spatio-temporal shape changes, dependent on their location and current role. Their morphology can range from highly branched, ramified cells with small cell bodies to ameboid, rounded cells with large cell bodies. When microglia are dormant, they have a lot of branches to survey the microenvironment; when they become activated and secrete pro-inflammatory cytokines, their morphology changes to ameboid by reorganizing proteins of the cell skeleton (actin, vimentin and microtubules)[64–66]. Here, an increased fraction of ameboid cells was observed after PapRIV treatment which is thus an additional proof of the microglia activating properties of this QSP. The effects are mediated by an NF-κB-dependent pathway, an increased nuclear translocation of NF-κB is observed which is caused by activation of the canonical pathway as a decrease of IκBα, a cytoplasmic inhibitory protein of NF-κB, and no NIK expression (data not shown) is seen[67]. When treating SH-SY5Y neuroblast cells with PapRIV conditioned BV-2 medium, toxic effects were seen at the higher PapRIV concentrations. Indeed, when treating SH-SY5Y cells with conditioned medium from activated BV-2 cells a decrease in viability is observed[68]. Several neurotoxic factors such as pro-inflammatory cytokines and extracellular ROS have been identified which may play a role in this microglia-mediated neurotoxicity[69]. Direct peptide treatment of the neuroblast cells did not result in a decreased viability, indicating that the toxic effects are mediated by the microglial activation. These results indicate the potential involvement of the peptide in microglia-mediated neurodegeneration.

To investigate the structure–activity relationship of the peptide, an alanine-scan was synthesized. By alternately replacing every amino acid with an alanine residue, crucial amino acids of the peptide can be identified. It is demonstrated that the second (aspartic acid) and the fourth (proline) amino acid are crucial for the peptide to exert its microglia activating effects. A scrambled control peptide of the sequence did not show any activating effects; indicating that the specific peptide sequence is responsible for the pro-inflammatory actions.

Different metabolites of the peptide were ex vivo identified in different tissues with DLPFEH being the main metabolite which is formed in all tissues (serum, brain, liver, kidney and faeces). This metabolite contains the two critical amino acids and our experiment demonstrated that it remains active, thus contributing to PapRIV-mediated microglial activation. Two other metabolites, i.e. SDLPF and DLPF which are formed in serum, also contain the two critical amino acids, but are no longer active. Since SDLPFE, which is not identified as a metabolite, still remains active (data not shown), it is hypothesized that the peptide needs a minimal length of six amino acids to exert its effects. The half-live of the peptide varies from 20 min in kidney tissue to 523 min in brain tissue. In serum, a half-live of 25 min is observed. The differences observed between the tissues are due to the high concentration of proteases in serum and the renal brush border membrane, while in colon tissue, a much lower expression of brush border enzymes is observed[70]. Using PeptideCutter and PROSPER, an in silico prediction of the potential responsible proteases for the observed metabolites was made[71]. DLPFEH can be formed by cleavage of Asp-N endopeptidases at position 1 and DLPF due to an extra cleavage at position 5 by chymotrypsin or proteinase K. SDLPF can be formed by actions of chymotrypsin or proteinase K at position 5, while LPFE can be formed by the simultaneous action of formic acid at position 2 and glutamyl endopeptidase or matrix-metalloprotease 9 (MMP 9) at position 6. Finally, LPF can be formed directly by the combined actions of formic acid and proteinase K or chymotrypsin (Table 4).

While we have shown the possible role of quorum sensing peptides as part of the microbiome as one of the causative factors in the gut-brain axis, further research is warranted. First, it remains to be demonstrated whether presence of PapRIV producing bacterial species in the gastro-intestinal tract results in sufficient QSP concentrations in the brain to exert effects on microglia. Next, effects of the peptide on the peripheral immune system need to be investigated as peripheral inflammation can also have a negative effect on the brain and blood–brain barrier integrity. In addition, in-vivo animal studies are required to confirm the observed in vitro effects. Finally, towards translational diagnostic and/or therapeutic use in humans, the presence of this QSP in faeces and/or plasmain humans (and more specifically in patients) is currently ongoing.

Matrix	Cleavage sites	Proteases
Serum	S|D|LPF|E|H	Asp-N endopeptidase, formic acid, chymotrypsin, proteinase K, glutamyl endopeptidase, MMP 9
Liver	S|D|LPFEH	Asp-N endopeptidase, formic acid
Brain	S|D|LPFEH	Asp-N endopeptidase, formic acid
Kidney	S|D|LPF|EH	Asp-N endopeptidase, formic acid, chymotrypsin, proteinase K
Faeces	S|DLPFEH	Asp-N endopeptidase

Table 4. Overview of cleavage sites and in silico predicted responsible proteases.

Conclusion

PapRIV, a QSP produced by members of the *B. cereus* group, shows in vitro activating properties towards BV-2 microglia cells. This QSP is produced in the gut and is able to cross the Caco-2 intestinal cell model via passive paracellular diffusion. Once reaching the circulation, it is able to cross the blood–brain barrier and reach the brain parenchyma. Presence of this QSP in mouse plasma was demonstrated for the first time. The peptide induces the expression of pro-inflammatory cytokines (IL-6 and TNFα) and ROS, and increases the fraction of ameboid cells via an NF-κB-dependent pathway in BV-2 microglia cells. Treatment of SH-SY5Y neuroblast cells with PapRIV conditioned BV-2 medium results in a decreased viability of these neuroblastoma cells, indicating indirect microglia-mediated neurotoxic effects of the peptide.

Overall, our in vitro obtained findings indicate for the first time a possible role of this bacterial quorum sensing peptide in gut-to-brain signaling, opening new avenues investigating their translational relevance.

Materials and methods

Peptides and reagents. Synthetic PapRIV was purchased from GL Biochem (Shanghai, China). The alanine scan, metabolites and scrambled control were synthesized using solid-phase peptide synthesis (Supplementary method S1). The quality of all peptides was determined using an in-house developed QC method and a purity of 95% or more was found for each sequence. Calcium dichloride dihydrate, magnesium sulphate, potassium chloride, sodium dihydrogen phosphate hydrate, HEPES, sodium lactate and urethane were purchased from Sigma-Aldrich (Diegem, Belgium), while Bovine Serum Albumin (BSA), sodium iodide, sodium dihydrogen phosphate monohydrate were obtained from Merck KGaA (Darmstadt, Germany). Sodium chloride and disodium hydrogen phosphate dihydrate were obtained from VWR (Leuven, Belgium). Calcium dichloride and D-glucose were purchased from Fluka (Diegem, Belgium) and dextran from AppliChem GmbH (Darmstadt, Germany). Water was purified using an Arium 611 Pro VF purification system (Sartorius, Göttingen, Germany) to laboratory-graded water (18.2 MΩ × cm).

Animals. Female, Institute for Cancer Research, Caesarean Derived-1 (ICR-CD-1) mice (Envigo, Venray, The Netherlands) of age 7–10 weeks and weighing 26–30 g, were used during the blood–brain barrier (BBB) transport experiments and C57Bl6/J WT mice, aged 3–24 months, were used for detection of PapRIV in plasma. Feed and water were provided ad libitum. All animal experiments were performed in strict accordance with the Belgian legislation RD 31/12/2012 and the Ethical Committee principles of laboratory animal welfare; the protocols were approved by the Ethical Committee of Ghent University, Faculties of Veterinary Medicine and Medicine and Health Sciences (approval numbers 2014-128 and ECD 19-17). All authors complied with the ARRIVE guidelines.

Cells. BV-2 cells were a kind gift from Prof. Alba Minelli and were grown in RPMI medium supplemented with 10% fetal bovine serum (FBS) and 1% penicillin-streptromycin solution (Life Technologies, Belgium). The cells were cultured in culture flasks (Greiner, Belgium) in an incubator set at 37 °C and 5% CO_2. When confluent, cells were detached using a cell scraper and diluted 1:20 approximately every 4 days. Experiments were performed in serum-free DMEM without phenol red.

SH-SY5Y neuroblast cells (Sigma-Aldrich, Diegem, Belgium) were grown in F12:MEM (50/50 v/v) medium supplemented with 15% FBS, 1% non-essential amino acids (NEAA), 2 mM $_L$-Glutamine and 1% penicillin/streptomycin solution (Life Technologies, Belgium) in an incubator set at 37 °C and 5% CO_2. When confluent, cells were detached using 0.25% Trypsin–EDTA.

Caco-2 assay. Caco-2 (Sigma-Aldrich, Diegem, Belgium) cells were grown in DMEM supplemented with 10% FBS, 1% NEAA and 1% penicillin/streptomycin solution. A total of 3×10^5 cells per filter were seeded in a 12-well plate and left for differentiation during 21–29 days (medium change every other day). Monolayer formation was checked by measuring the TEER values which should be above 0.30 kΩ × cm^2 [72]. After washing with Hank's balanced salt solution, 400 µL of a 1 µM peptide solution was added to the apical side of the filter. After 30, 60, 90 and 120 min, 100 µL of the acceptor compartment was taken for UPLC-MS/MS analysis (Supplementary method S2). Linear curve fitting was used to calculate the apparent permeability coefficient (P_{app}), as sink

conditions were achieved. The P_{app} was determined from the amount of peptide transported per time unit and calculated using the following equation:

$$P_{app} = \left(\frac{dQ}{dt}\right) \times \left(\frac{1}{A \times C_0}\right) \quad (1)$$

with dQ/dt = the steady-state flux (pM/s), experimentally obtained; A = the surface area of the filter (= 1.12 cm^2); C_0 = the initial concentration in the donor compartment (= 1×10^6 pM).

The reduction in acceptor concentration was also taken into account after every sampling. The cumulative amount in the acceptor compartment is defined as:

$$Cumulative\ amount = C_{r_n} V_r + \sum_{k=1}^{n-1} C_{r_k} V_s \quad (2)$$

with C_{r_k} = concentration at sample point k in acceptor compartment; V_r = volume in the receiver chamber; V_s = volume sampled; n = times sampled.

Detection of PapRIV in mouse plasma. Sixty µL of mouse plasma was used for the detection of PapRIV and prepared using solid-phase extraction (SPE). Mouse plasma was mixed with an ACN/DMSO mixture acidified with FA (94/3/3 V/V). After 30 s vortexing and sonification (30 s), the sample was boiled for 1 min at 100 °C followed by centrifugation (30 s, 10,000*g*). One hundred µL of the supernatant was then mixed with 800 µL ACN/DMSO mixture (97/3 V/V) acidified with 0.1% FA. This sample was then loaded on a MonoSpin Amide SPE column (GL Sciences Inc., Japan) conditioned with a water/ACN mixture (90/10 V/V) basified with 0.1% NH_4OH and equilibrated with the same ACN/DMSO mixture. The sample was eluted using a water/ACN/DMSO mixture (75/20/5 V/V) acidified with 0.1% FA. The eluent was brought into vials which were coated with an albumin based anti-adsorption solution, which considerably decreases the adsorption to glass for certain peptides and improves the overall sensitivity of the method[73]. Ten µL of the eluent was injected on an Acquity UPLC BEH C18 (2.1 × 100 mm; 1.7 µm) column equipped with a guard column. Column temperature was maintained at 60 °C. Mobile phase A consisted of water/ACN/DMSO (93/2/5 V/V) + 0.1% FA, Mobile phase B consisted of water/ACN/DMSO (2/93/5 V/V) + 0.1% FA. A gradient ranging from 100% mobile phase A to 60% mobile phase B over 12 min was used. MS analysis was performed using a Quadrupole-Time-of-flight system (SYNAPT G2-Si) (Waters, Milford, USA) for identification purposes and a triple Quadrupole system (Xevo) (Waters, Milford, USA) for quantification, both with electrospray ionisation set in positive mode. Ionization was conducted using a needle voltage of 3.0 kV, a cone voltage of 20 V and a source temperature of 120 °C. Nitrogen was used as sheath and auxiliary gas at a temperature of 500 °C. Argon was used as collision gas at an energy of 32 V. Detection was performed using a fixed mass and collision energy on the first quadrupole set on the mother ion (844.35 ± 0.5 *m/z*) and MS/MS acquisition over the 100–1450 *m/z* range using the second TOF analyser, while quantification with triple quadrupole used the product ions *m/z* 529.2 and 642.3. Samples were considered positive identified when a signal appeared at the expected retention time (Δ < 1%) and when at least three identification ions (one parent ion and two daughter ions) of the peptide were found[74]. Quantification on the triple quadrupole was done above the reporting threshold of 1.5 nM concentrations and using a 10 nM spiked placebo sample as reference.

Peptide ^{125}I radiolabelling. PapRIV and the controls BSA and dermorphin (Hanhong, Shanghai, China) were iodinated using the Iodo-Gen method as previously described[75]. Briefly, 0.1 µmol of the lyophilized peptide was dissolved in 100 µL of phosphate buffer (pH 7.4, 25 mM). A Iodo-Gen coated tube (Thermo Scientific, Merelbeke, Belgium) was first of all rinsed with 1 mL of phosphate buffer. Subsequently, 50 µL of sodium iodide solution (1.1 µmol/mL) and 1 mCi of $Na^{125}I$ solution (Perking Elmer, Zaventem, Belgium) were transferred into this Iodo-Gen coated tube. The oxidation reaction was allowed to proceed for six minutes at room temperature, after which the iodonium solution was transferred to 50 µL of peptide solution (1 mM). The iodination reaction of the peptide was allowed to proceed for another six minutes at room temperature. Finally, the iodinated peptide was purified using a silver filter (Thermo Scientific, Merelbeke, Belgium).

Multiple time regression analysis. In order to determine whether the peptide could enter the brain, in vivo multiple time regression (MTR) analysis was performed. ICR-CD-1 mice were anesthetized intraperitoneally using a 40% urethane solution (3 g/kg). Then, the jugular vein and carotid artery were isolated and 200 µL of the radiolabeled peptide solution, diluted to 30,000 cpm/µL using Lactated Ringer's solution containing 1% of BSA (LR/BSA), was injected into the jugular vein. At specified time points after injection (i.e. 1, 3, 5, 10, 12.5 and 15 min, with start and end in duplicate), blood was obtained from the carotid artery followed by decapitation of the mouse. The isolated brain was weighed and radioactivity measured in a gamma counter for 5 min (Wallac Wizard automatic gamma counter, Perkin Elmer, Shelton, CT, USA), as well as from 50 µL serum, which was obtained by centrifuging the collected blood at 10,000*g* for 15 min at 21 °C. The linear and biphasic modeling of the multiple time regression analysis was performed as previously described[14].

Capillary depletion. We performed capillary depletion to determine whether the peptides, taken up by the brain, completely crossed the capillary wall into the tissue rather than just being trapped by and in the endothelium. The method of Triguero et al., as modified by Gutierrez et al., was used[76,77]. ICR-CD-1 mice were first anesthetized intraperitoneally using a 40% urethane solution (3 g/kg). After isolation of the jugular vein, 200 µL

Gene	Supplier	Sequence (5′ → 3′)
IL-6	Invitrogen	Fw: ACCACTTCACAAGTCGGAGGC Rev: CTGCAAGTGCATCATCGTTGTTC
Ppia	Qiagen	–[a]
Rer	Invitrogen	Fw: AGTGGATCCTTCCTTGATGG Rev: ATGCCTTTTGTAGCTGCG

Table 5. Primers for BV-2 qPCR. [a]Sequence of the primers is not disclosed by Qiagen.

of the iodinated peptide solution, diluted to 10,000 cpm/µL using LR/BSA, was injected in the jugular vein. Ten minutes after injection, blood was collected from the abdominal aorta and the brain was perfused manually with 20 mL of Lactated Ringer's buffer after clamping the aorta and severing the jugular veins. Subsequently, the brain was collected, weighed and the radioactivity measured in the gamma counter for 5 min. Then, the brain was homogenized with 0.7 mL of ice-cold capillary buffer (10 mM HEPES, 141 mM NaCl, 4 mM KCl, 2.8 mM $CaCl_2$, 1 mM $MgSO_4$, 1 mM NaH_2PO_4 and 10 mM D-glucose adjusted to pH 7.4) in a pyrex glass tube and mixed with 1.7 mL of 26% ice-cold dextran solution in capillary buffer. The resulting solution was weighed and centrifuged in a swinging bucket rotor at 5400*g* for 30 min at 4 °C, after measuring the radioactivity in the gamma counter. Pellet (capillaries) and supernatant (parenchyma and fat tissues) were also collected, weighed and measured in a gamma counter. After centrifuging the obtained blood (10,000*g*, 21 °C, 15 min), the radioactivity of 50 µL serum was measured in a gamma counter as well.

Brain-to-blood transport. We quantified the amount of peptide exported out of the brain as previously described[78]. ICR-CD-1 mice were anesthetized intraperitoneally using a 40% urethane solution (3 g/kg). Then, the skin of the skull was removed and using a 22 G needle marked with tape at 2 mm, a hole was made into the lateral ventricle at the following coordinates: 1 mm lateral and 0.34 mm posterior to the bregma. The anesthetized mice received an intracerebroventricular (ICV) injection of 1 µL of the diluted iodinated peptide solution using LR/BSA (25,000 cpm/µL) by pumping the peptide solution at a speed of 360 µL/h for 10 s using a syringe pump (KDS100, KR analytical, Cheshire, UK). At specified time points after ICV-injection (i.e. 1, 3, 5, 10, 12.5 and 15 min), blood was collected from the abdominal aorta and subsequently the mouse was decapitated. Then, the whole brain was collected, weighed and measured in a gamma counter for 5 min. Fifty µL of serum, which was obtained by centrifuging the collected blood at 10,000*g* during 15 min at 21 °C, and the background was also measured in a gamma counter. The efflux half-life was calculated from the linear regression of the natural logarithm of the residual radioactivity in brain versus time as follows:

$$t_{1/2} = \frac{\ln(2)}{k_{out}} \tag{3}$$

where k_{out} is defined as the efflux rate constant calculated as the negative value of the slope of the linear regression, applying first order kinetics.

IL-6 and TNFα determination. To investigate the microglia activating properties of the peptide, IL-6 and TNFα levels were determined in cell-free supernatants of BV-2 microglia cells after treatment. BV-2 cells (2×10^5 cells/well) were seeded in 24-well plates and treated with peptide for 20 h. ELISA was performed according to the supplier's protocol (eBioscience, Vienna, Austria). Briefly, after incubation with biotinylated detection antibody, avidin-HRP conjugate and subsequently chromogenic tetramethylbenzidine (TMB) substrate were added. Absorbance was measured at 450 nm and 570 nm using the Multiskan Ascent 354 microplate reader (Thermofisher, Waltham, USA). Concentrations were determined using the standard curve generated using known concentrations of TNFα and IL-6.

qPCR. To confirm the observed ELISA results at mRNA level, a qPCR experiment was performed. After incubation of the BV-2 cells with PapRIV or controls, cells were lysed in RLT buffer (Qiagen, Hilden, Germany) supplemented with 1% β-mercaptoethanol. The lysate was stored at − 80 °C until RNA extraction. RNA was extracted using the RNeasy Mini Kit (Qiagen, Hilden, Germany). DNAse steps were included in the protocol to remove possible DNA contamination. RNA purity and concentration were assessed using spectrophotometry (NanoDrop), while RNA quality was evaluated using capillary electrophoresis (Fragment Analyzer). After extraction, the RNA was immediately converted to cDNA which was stored at − 20 °C until qPCR analysis. Ppia and Rer were chosen as suitable control genes based on the GeNorm and Normfinder algorithms[79,80]. Used primers are given in Table 5. qPCR cycling was performed using a LightCycler 480 (Roche), with Cq values being calculated using the second derivative threshold method.

ROS assay. Microglia activation is accompanied by an increased reactive oxygen species (ROS) production. The ROS assay was performed using a fluorometric intracellular ROS kit according to the supplier's protocol (Sigma-Aldrich, Diegem, Belgium). In brief, 4×10^4 cells/well were seeded in a black 96-well plate. Four hours post seeding, 100 µL of master reaction mix was added to the wells and incubated for 1 h after which cells were treated with PapRIV dissolved in PBS for 24 h. Fluorescence intensity was measured using an EnVision fluorometric plate reader at $\lambda_{ex} = 492/\lambda_{em} = 535$ nm (Perkin Elmer, Zaventem, Belgium).

Morphological analysis. We investigated the morphology since microglia change their morphology from a branched structure to a more round, ameboid structure after activation. BV-2 cells were seeded in 1×10^4 cells/well in a 24-well plate (360 µL); this way direct cell–cell contacts, which have an influence on morphology, are avoided. Four hours post-seeding, cells were treated with 40 µL peptide, placebo (H_2O), medium or positive control (LPS 1 µg/mL). For the assessment of the morphology, one picture in the center of each well (100 × magnification) was taken after twenty hours with an Olympus CKX53 phase-contrast microscope equipped with an XC30 CCD camera (Olympus NV, Antwerp, Belgium). The number of branched and ameboid cells was counted with the cell counter plugin of ImageJ.

Immunoblotting. To assess nuclear translocation of NF-kB, cells were lysed after 20 h using the NE-PER protocol (Thermo Scientific). Using this kit, the cytoplasmic and nuclear protein fractions are separated from each other. To asses IκBα expression, cells were lysed with RIPA buffer. Protein content of the lysates was determined using the modified Lowry assay (Thermo Scientific). Proteins (20 µg) were separated using an Any kD gel (SDS-PAGE) and transferred to a nitrocellulose membrane (BioRad, Temse, Belgium). Aspecific binding sites were blocked for 30 min using TBS + 1% casein (BioRad, Temse, Belgium). Western blot was performed using the following primary polyclonal antibodies overnight (4 °C): anti-p65 NFkB (1/500), anti-IκBα (1/1000) and anti-β-actin (1/1000), β-tubulin (1/4000) and anti-Histon H3.3 (1/5000) were used as loading controls. Goat anti-rabbit-AP antibody was used for detection (1/10,000) (60 min). All antibodies were purchased at Thermo Scientific (Merelbeke, Belgium). Finally, the BCIP/NBT substrate was added and the results were analyzed using the GelDoc EZ imager and Image Lab software (BioRad, Temse, Belgium). TBS buffer was used for washing between the steps.

MTT assay. SH-SY5Y cells were seeded at a density of 5×10^4 cells/well in a 96-well plate and incubated for 24 h. Next, medium was removed and replaced by 200 µL conditioned medium of BV-2 cells which were treated for 20 h with PapRIV. After 24 h incubation, 20 µL MTT reagent (12 mM) was added and incubated for 3 h. Finally, the medium was removed and replaced by 150 µL DMSO and measured at 570 nm with a microplate reader (Thermofisher, Waltham, USA).

Ex vivo metabolization. Peptide solution (0.1 mg/mL) was incubated with serum, brain, liver, kidney, colon or faeces homogenate at 37 °C. After 0, 5, 10, 30 and 60 min, aliquots were taken for UPLC-UV/MS analysis. Preparation of the tissue homogenates and UPLC-UV/MS parameters are given in supplementary information (Supplementary methods S3-S4). The half-live was calculated using the following equation:

$$T_{1/2} = \frac{-\ln(2)}{Slope} \tag{4}$$

where the slope is defined by linear regression assuming first order kinetics.

Statistical analysis. Statistical analysis of PapRIV treated cells compared to vehicle treated cells was performed using one-way ANOVA; the Dunnett test was performed to adjust for multiple comparisons with the control group (placebo). A p value of < 0.05 was considered significant. The Mann–Whitney U test was used for the qPCR experiment. Linear and biphasic modelling was applied for the MTR experiments as described by Wynendaele et al.[14]. For the efflux and Caco-2 experiment, regular linear regression was applied. Data are expressed as mean ± SEM unless otherwise specified. Statistical analysis was performed and graphs were made using Graphpad Prism 6 (Graphpad Software, La Jolla, USA).

Ddata availability

The data that support the findings of this study are available on request from the corresponding author. The data are not publicly available due to privacy or ethical restrictions.

Received: 15 January 2021; Accepted: 6 May 2021
Published online: 21 May 2021

References

1. Miller, M. B. & Bassler, B. L. Quorum sensing in bacteria. *Annu. Rev. Microbiol.* **55**, 165–199 (2001).
2. Albuquerque, P. & Casadevall, A. Quorum sensing in fungi—a review. *Med. Mycol.* **50**(4), 337–345 (2012).
3. Yashiroda, Y. & Yoshida, M. Intraspecies cell-cell communication in yeast. FEMS Yeast Res. 19(7), foz071 (2019)
4. Debunne, N., Verbeke, F., Janssens, Y., Wynendaele, E. & De Spiegeleer, B. Chromatography of quorum sensing peptides: an important functional class of the bacterial peptidome. *Chromatographia* **81**(1), 25–40 (2018).
5. Papenfort, K. & Bassler, B. L. Quorum sensing signal-response systems in Gram-negative bacteria. *Nat. Rev. Microbiol.* **14**(9), 576–588 (2019).
6. Verbeke, F. *et al.* Peptides as quorum sensing molecules: measurement techniques and obtained levels in vitro and in vivo. *Front. Neurosci.* **11**, 183 (2017).
7. Herzog, R., Peschek, N., Frohlich, K. S., Schumacher, K. & Papenfort, K. Three autoinducer molecules act in concert to control virulence gene expression in *Vibrio cholerae*. *Nucleic Acids Res.* **47**(6), 3171–3183 (2019).
8. Pesci, E. C. *et al.* Quinolone signaling in the cell-to-cell communication system of *Pseudomonas aeruginosa*. *Proc. Natl. Acad. Sci. U S A.* **96**(20), 11229–11234 (1999).
9. Wynendaele, E. *et al.* Quorumpeps database: chemical space, microbial origin and functionality of quorum sensing peptides. *Nucleic Acids Res.* **41**(Database issue), D655–D659 (2013).

10. De Spiegeleer, B. *et al.* The quorum sensing peptides PhrG, CSP and EDF promote angiogenesis and invasion of breast cancer cells in vitro. *PLoS ONE* **10**(3), e0119471 (2015).
11. Wynendaele, E. *et al.* Crosstalk between the microbiome and cancer cells by quorum sensing peptides. *Peptides* **64**, 40–48 (2015).
12. Pundir, P. *et al.* A connective tissue mast-cell-specific receptor detects bacterial quorum-sensing molecules and mediates antibacterial immunity. *Cell Host Microbe.* **26**(1), 114-122e8 (2019).
13. De Spiegeleer, A. *et al.* Quorum sensing molecules as a novel microbial factor impacting muscle cells. *Biochim. Biophys. Acta Mol. Basis Dis.* **1866**(3), 165646 (2020).
14. Wynendaele, E. *et al.* Quorum sensing peptides selectively penetrate the blood–brain barrier. *PLoS ONE* **10**(11), e0142071 (2015).
15. Janssens, Y. *et al.* Screening of quorum sensing peptides for biological effects in neuronal cells. *Peptides* **101**, 150–156 (2018).
16. Barichella, M. *et al.* Unraveling gut microbiota in Parkinson's disease and atypical parkinsonism. *Mov. Disord.* **34**(3), 396–405 (2019).
17. Janssens, Y. *et al.* Disbiome database: linking the microbiome to disease. *BMC Microbiol.* **18**(1), 50 (2018).
18. Strati, F. *et al.* New evidences on the altered gut microbiota in autism spectrum disorders. *Microbiome* **5**(1), 24 (2017).
19. Vogt, N. M. *et al.* Gut microbiome alterations in Alzheimer's disease. *Sci. Rep.* **7**(1), 13537 (2017).
20. Xu, R., Wu, B., Liang, J., He, F., Gu, W., Li, K., et al. Altered gut microbiota and mucosal immunity in patients with schizophrenia. Brain Behav Immun. 85, 120-127 (2020).
21. Chen, J. J. *et al.* Age-specific differential changes on gut microbiota composition in patients with major depressive disorder. *Aging* **12**(3), 2764–2776 (2020).
22. Panza, F., Lozupone, M., Solfrizzi, V., Watling, M. & Imbimbo, B. P. Time to test antibacterial therapy in Alzheimer's disease. *Brain* **142**(10), 2905–2929 (2019).
23. Valles-Colomer, M. *et al.* The neuroactive potential of the human gut microbiota in quality of life and depression. *Nat. Microbiol.* **4**(4), 623–632 (2019).
24. Zhu, F. *et al.* Metagenome-wide association of gut microbiome features for schizophrenia. *Nat. Commun.* **11**(1), 1612 (2020).
25. Sampson, T. R. *et al.* Gut microbiota regulate motor deficits and neuroinflammation in a model of Parkinson's disease. *Cell* **167**(6), 1469-1480 e12 (2016).
26. Shen, H. *et al.* New mechanism of neuroinflammation in Alzheimer's disease: The activation of NLRP3 inflammasome mediated by gut microbiota. *Prog. Neuropsychopharmacol. Biol. Psychiatry.* **100**, 109884 (2020).
27. Tengeler, A. C. *et al.* Gut microbiota from persons with attention-deficit/hyperactivity disorder affects the brain in mice. *Microbiome* **8**(1), 44 (2020).
28. Kim, M. S. *et al.* Transfer of a healthy microbiota reduces amyloid and tau pathology in an Alzheimer's disease animal model. *Gut* **69**(2), 283–294 (2020).
29. Dinan, T. G. & Cryan, J. F. The microbiome-gut-brain axis in health and disease. *Gastroenterol. Clin. N. Am.* **46**(1), 77–89 (2017).
30. Cryan, J. F. *et al.* The microbiota-gut-brain axis. *Physiol Rev.* **99**(4), 1877–2013 (2019).
31. Lach, G., Schellekens, H., Dinan, T. G. & Cryan, J. F. Anxiety, depression, and the microbiome: a role for gut Peptides. *Neurotherapeutics* **15**(1), 36–59 (2018).
32. Abdel-Haq, R., Schlachetzki, J. C. M., Glass, C. K. & Mazmanian, S. K. Microbiome-microglia connections via the gut-brain axis. *J. Exp. Med.* **216**(1), 41–59 (2019).
33. Chu, F. *et al.* The roles of macrophages and microglia in multiple sclerosis and experimental autoimmune encephalomyelitis. *J. Neuroimmunol.* **318**, 1–7 (2018).
34. Geloso, M. C. *et al.* The dual role of microglia in ALS: mechanisms and therapeutic approaches. *Front Aging Neurosci.* **9**, 242 (2017).
35. Koyama, R. & Ikegaya, Y. Microglia in the pathogenesis of autism spectrum disorders. *Neurosci. Res.* **100**, 1–5 (2015).
36. Xiang, Z., Haroutunian, V., Ho, L., Purohit, D. & Pasinetti, G. M. Microglia activation in the brain as inflammatory biomarker of Alzheimer's disease neuropathology and clinical dementia. *Dis. Markers.* **22**(1–2), 95–102 (2006).
37. Yin, Z. *et al.* Immune hyperreactivity of Abeta plaque-associated microglia in Alzheimer's disease. *Neurobiol. Aging.* **55**, 115–122 (2017).
38. Erny, D. *et al.* Host microbiota constantly control maturation and function of microglia in the CNS. *Nat. Neurosci.* **18**(7), 965–977 (2015).
39. Wang, X. *et al.* Sodium oligomannate therapeutically remodels gut microbiota and suppresses gut bacterial amino acids-shaped neuroinflammation to inhibit Alzheimer's disease progression. *Cell Res.* **29**(10), 787–803 (2019).
40. Ceuppens, S., Boon, N. & Uyttendaele, M. Diversity of Bacillus cereus group strains is reflected in their broad range of pathogenicity and diverse ecological lifestyles. *FEMS Microbiol Ecol.* **84**(3), 433–450 (2013).
41. Bouillaut, L. *et al.* Molecular basis for group-specific activation of the virulence regulator PlcR by PapR heptapeptides. *Nucleic Acids Res.* **36**(11), 3791–3801 (2008).
42. Pomerantsev, A. P. *et al.* PapR peptide maturation: role of the NprB protease in *Bacillus cereus* 569 PlcR/PapR global gene regulation. *FEMS Immunol. Med. Microbiol.* **55**(3), 361–377 (2009).
43. Slamti, L. & Lereclus, D. A cell-cell signaling peptide activates the PlcR virulence regulon in bacteria of the Bacillus cereus group. *Embo J.* **21**(17), 4550–4559 (2002).
44. Grenha, R. *et al.* Structural basis for the activation mechanism of the PlcR virulence regulator by the quorum-sensing signal peptide PapR. *Proc. Natl. Acad. Sci. U S A.* **110**(3), 1047–1052 (2013).
45. Stalmans, S. *et al.* Classification of peptides according to their blood–brain barrier influx. *Protein Pept. Lett.* **22**(9), 768–775 (2015).
46. Blasi, E., Barluzzi, R., Bocchini, V., Mazzolla, R. & Bistoni, F. Immortalization of murine microglial cells by a v-raf/v-myc carrying retrovirus. *J Neuroimmunol.* **27**(2–3), 229–237 (1990).
47. Henn, A. *et al.* The suitability of BV2 cells as alternative model system for primary microglia cultures or for animal experiments examining brain inflammation. *Altex* **26**(2), 83–94 (2009).
48. Timmerman, R., Burm, S. M., & Bajramovic, J. J. An overview of in vitro methods to study microglia. *Front Cell Neurosci*. **12**(242) (2018).
49. Shih, R. H., Wang, C. Y. & Yang, C. M. NF-kappaB signaling pathways in neurological inflammation: a mini review. *Front. Mol. Neurosci.* **8**, 77 (2015).
50. Brewis, I. A., Howell, S., Hooper, N. M., Kenny, A. J., & Turner, A. J. Membrane peptidase expression by confluent cultures of Caco-2 cells. *Biochem. Soc. Trans.* **21(Pt 3)**(3), 252s (1993).
51. Howell, S., Brewis, I. A., Hooper, N. M., Kenny, A. J. & Turner, A. J. Mosaic expression of membrane peptidases by confluent cultures of Caco-2 cells. *FEBS Lett.* **317**(1–2), 109–112 (1993).
52. Ceuppens, S. *et al.* Survival of *Bacillus cereus* vegetative cells and spores during in vitro simulation of gastric passage. *J. Food Prot.* **75**(4), 690–694 (2012).
53. Ceuppens, S. *et al.* Impact of intestinal microbiota and gastrointestinal conditions on the in vitro survival and growth of *Bacillus cereus*. *Int. J. Food Microbiol.* **155**(3), 241–246 (2012).
54. Tam, N. K. *et al.* The intestinal life cycle of *Bacillus subtilis* and close relatives. *J. Bacteriol.* **188**(7), 2692–2700 (2006).
55. Turnbull, P. C. & Kramer, J. M. Intestinal carriage of *Bacillus cereus*: faecal isolation studies in three population groups. *J. Hyg.* **95**(3), 629–638 (1985).
56. Bischoff, S. C. *et al.* Intestinal permeability—a new target for disease prevention and therapy. *BMC Gastroenterol.* **14**, 189 (2014).

57. Moravek, M. *et al.* Determination of the toxic potential of *Bacillus cereus* isolates by quantitative enterotoxin analyses. *FEMS Microbiol. Lett.* **257**(2), 293–298 (2006).
58. Shinagawa, K., Ueno, S., Konuma, H., Matsusaka, N. & Sugii, S. Purification and characterization of the vascular permeability factor produced by *Bacillus cereus*. *J. Vet. Med. Sci.* **53**(2), 281–286 (1991).
59. Bottone, E. J. Bacillus cereus, a volatile human pathogen. *Clin. Microbiol. Rev.* **23**(2), 382–398 (2010).
60. Asbjornsdottir, B. *et al.* Zonulin-dependent intestinal permeability in children diagnosed with mental disorders: a systematic review and meta-analysis. *Nutrients* **12**(7), 1982 (2020).
61. Kılıç, F., Işık, Ü., Demirdaş, A., Doğuç, D. K. & Bozkurt, M. Serum zonulin and claudin-5 levels in patients with bipolar disorder. *J. Affect Disord.* **266**, 37–42 (2020).
62. Bordt, E. A. & Polster, B. M. NADPH oxidase- and mitochondria-derived reactive oxygen species in proinflammatory microglial activation: a bipartisan affair?. *Free Radic. Biol. Med.* **76**, 34–46 (2014).
63. Yang, D. *et al.* Pro-inflammatory cytokines increase reactive oxygen species through mitochondria and NADPH oxidase in cultured RPE cells. *Exp. Eye Res.* **85**(4), 462–472 (2007).
64. Abd-el-Basset, E. & Fedoroff, S. Effect of bacterial wall lipopolysaccharide (LPS) on morphology, motility, and cytoskeletal organization of microglia in cultures. *J. Neurosci. Res.* **41**(2), 222–237 (1995).
65. Colton, C. & Wilcock, D. M. Assessing activation states in microglia. *CNS Neurol. Disord. Drug Targets* **9**(2), 174–191 (2010).
66. McHugh, D., Roskowski, D., Xie, S. & Bradshaw, H. B. Delta(9)-THC and N-arachidonoyl glycine regulate BV-2 microglial morphology and cytokine release plasticity: implications for signaling at GPR18. *Front. Pharmacol.* **4**, 162 (2014).
67. Moynagh, P. N. The NF-kappaB pathway. *J. Cell Sci.* **118**(Pt 20), 4589–4592 (2005).
68. Kwon, S. J., Ahn, T. B., Yoon, M. Y. & Jeon, B. S. BV-2 stimulation by lactacystin results in a strong inflammatory reaction and apoptotic neuronal death in SH-SY5Y cells. *Brain Res.* **1205**, 116–121 (2008).
69. Block, M. L. & Hong, J. S. Microglia and inflammation-mediated neurodegeneration: multiple triggers with a common mechanism. *Prog. Neurobiol.* **76**(2), 77–98 (2005).
70. Darmoul, D. *et al.* Regional expression of epithelial dipeptidyl peptidase IV in the human intestines. *Biochem. Biophys. Res. Commun.* **203**(2), 1224–1229 (1994).
71. Song, J. *et al.* PROSPER: an integrated feature-based tool for predicting protease substrate cleavage sites. *PLoS ONE* **7**(11), e50300 (2012).
72. Srinivasan, B. *et al.* TEER measurement techniques for in vitro barrier model systems. *J. Lab Autom.* **20**(2), 107–126 (2015).
73. Verbeke, F., Bracke, N., Debunne, N., Wynendaele, E. & De Spiegeleer, B. LC-MS compatible antiadsorption diluent for peptide analysis. *Anal Chem.* **92**(2), 1712–1719 (2020).
74. Mitrevski, B. S., Wilairat, P. & Marriott, P. J. Evaluation of World Anti-Doping Agency criteria for anabolic agent analysis by using comprehensive two-dimensional gas chromatography-mass spectrometry. *Anal Bioanal Chem.* **396**(7), 2503–2511 (2010).
75. Janssens, Y. *et al.* Analysis of iodinated quorum sensing peptides by LC-UV/ESI ion trap mass spectrometry. *J. Pharm. Anal.* **8**(1), 69–74 (2018).
76. Gutierrez, E. G., Banks, W. A. & Kastin, A. J. Murine tumor necrosis factor alpha is transported from blood to brain in the mouse. *J. Neuroimmunol.* **47**(2), 169–176 (1993).
77. Triguero, D., Buciak, J. & Pardridge, W. M. Capillary depletion method for quantification of blood–brain barrier transport of circulating peptides and plasma proteins. *J. Neurochem.* **54**(6), 1882–1888 (1990).
78. Banks, W. A. & Kastin, A. J. Quantifying carrier-mediated transport of peptides from the brain to the blood. *Methods Enzymol.* **168**, 652–660 (1989).
79. Andersen, C. L., Jensen, J. L. & Orntoft, T. F. Normalization of real-time quantitative reverse transcription-PCR data: a model-based variance estimation approach to identify genes suited for normalization, applied to bladder and colon cancer data sets. *Cancer Res.* **64**(15), 5245–5250 (2004).
80. Vandesompele, J. *et al.* Accurate normalization of real-time quantitative RT-PCR data by geometric averaging of multiple internal control genes. *Genome Biol.* **3**(7), research0034.1 (2002).

Acknowledgements

We thank Professor Alba Minelli for the kind gift of BV-2 cells.

Author contributions

Y.J., A.D.S., N.D. and E.W. performed the experiments. M.P. and L.F. performed the synthesis of the alanine-scan and metabolites. A.Q. and C.C. performed the iPSC experiments. Y.J., N.D., A.D.S. and B.D.S. analyzed data. Y.J., E.W., D.V.D., P.D.D., P.P., M.B.J. and B.D.S. designed the experiments. Y.J. and B.D.S. wrote the manuscript. The authors read and approved the final manuscript.

Funding

ND and ADS are supported by a grant of Research Foundation Flanders (FWO) (Grant Nos. 1S21017N and 1158818N respectively). Part of this work was financed by Grant MPCUdG2016/038 from the University of Girona. The funding bodies have no role in writing the manuscript.

Competing interests

The authors declare no competing interests.

Additional information

Supplementary Information The online version contains supplementary material available at https://doi.org/10.1038/s41598-021-90030-y.

Correspondence and requests for materials should be addressed to B.S.

Reprints and permissions information is available at www.nature.com/reprints.

Publisher's note Springer Nature remains neutral with regard to jurisdictional claims in published maps and institutional affiliations.